

Numerical study of polymer-induced drag reduction in flow past circular cylinder

Junfeng Yang^{1*}, Omar K. Matar¹

¹*Department of Chemical Engineering, Imperial College, London, SW7 2AZ, UK*

Abstract: Polymer-induced drag reduction takes the advantages of high efficiency for energy saving and consequently attracted a lot of research interest in recent decades. However, the interplays between polymer rheological parameters and drag reduction and flow features have not been explored extensively. In this study, a molecular-based non-Newtonian viscoelastic model, so-called, Finite Extendible Nonlinear Elastic-Peterlin (FENE-P) rheological model, has been incorporated into a 3D transient CFD code in order to investigate the polymer-induced drag-reduction in flow past cylinder over a wide range of rheological and flow parameters. The modeling results demonstrate that generally viscoelastic polymer solutions can indeed reduce the drag coefficient by means of the polymer stretch which facilitates the resistance on the wake instability. Particular attention has been paid to instantaneous vorticity fields, as well as the drag coefficient and vortices shedding frequency. It is found that the viscoelastic fluid flow elongates recirculation region behind the cylinder. The extent of drag reduction is elevated as polymer elasticity becomes stronger. However, the solution containing extreme long chain polymer might exhibit solid-like characteristics and cause the upstream pressure of cylinder increase, leading a larger drag on the cylinder. In addition, the simulations reveal that vortices shedding frequency are largely reduced by the viscoelasticity. These results are indicative of the predictive capability of established numerical model for viscoelastic fluid flow. The model is useful to explain the observations of polymer-induced drag reduction and gains insights into how polymeric additives can influence the flow features.

Keywords: drag reduction, turbulent flow, viscoelastic polymer

1 Introduction

Polymer additives are often used to reduce friction drag of wall-bounded turbulent flows. The flow of a polymer solution exhibiting viscoelastic property has been reported to reduce up to 80% frictional drag compared to that the equivalent flow of the pure solvent¹. Understanding of the role of polymers in the mechanism of drag reduction not only facilitates the development of advanced drag reduction models, but also provides valuable insights into turbulence itself. In the past half-century, numerous experimental and numerical studies have been conducted in order to better understand the origins of polymer-induced drag reduction, and various explanations have been proposed on the basis of their results. Broadly speaking, three classes of phenomenological explanation² have been put forward: polymers cause the

* **Corresponding author:** Junfeng Yang, Email: junfeng.yang@imperial.ac.uk.

buffer-layer thickness to extend across the entire boundary layer, polymers diminish the Reynolds stresses and polymers damp the streamwise vortices. Obviously, these studies provide the direct evidence that polymers alter turbulent flow structure. However, the fundamental principles underpinning this polymer-turbulence interaction remain elusive, and current experimental techniques (e.g. Particle Image Velocimetry, Phase Doppler Anemometry) have not yet proved to be sufficient for their identification³.

Consequently, computational modeling of non-Newtonian viscoelastic flow is an attractive tool for obtaining new insights into the polymer-induced drag reductions. The simplest model to describe the elastic behavior of a polymer molecular is the so-called Dumbbell model. This model approximates an individual member of a dilute concentration of polymers as a single dumbbell connected with a finitely extensible, nonlinear elastic spring, and through a balance of forces acting on the beads, see Fig. 1. The beads represent molecular segments of several monomers and the spring describes the entropic effects to which the end-to-end vector of the polymer is subject.

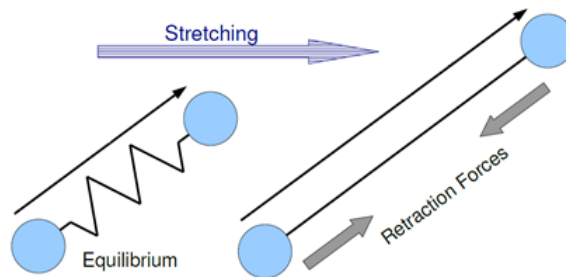


Figure 1 Schematic of dumbbell model for polymer molecular

Several dumbbell-concept-based constitutive models have been derived to predict the product of the aforementioned end-to-end vector, so-called conformation tensor. Among them are Upper-Convected Maxwell (UCM) model, Oldroyd-B model and finite-extensibility-nonlinear-elastic (FENE) model family including FENE-Peterlin closure (FENE-P)⁴, FENE- Chilcott-Rallison closure (FENE-CR)⁵ and modified FENE-CR⁶. The quasi-linear UCM and Oldroyd-B models do not consider the maximum extensibility of polymer, which limited the application to very low values of the Weissenberg number and polymer extensibility⁷. The FENE model family are improved version of Oldroyd-B model, where a maximum extensibility has been introduced to bound the extension of spring, and thus the bounded stress of the polymers. This feature allows capturing the basic rheological properties of a polymer solution.

The FENE model family has been widely verified over a wide range of rheological and flow parameters. Recent works on FENE model family are discussed herein. Richter et al. (2011)⁸ utilized a modified FENE-P rheological model to simulate viscoelastic flow past a cylinder at moderate Reynolds numbers. The predicted Strouhal number, drag coefficient and lengthening of the recirculation region were

compared against the previous experiments. The FENE-P constitutive equations have been embedded into an in-housed code to study the effects of viscoelasticity on the transitioning cylinder wakes. It has found FENE-P model show relatively good agreement with aforementioned FENE-MCR model for the drag and shedding frequency. It also reveals viscoelasticity reduces the vortex shedding frequency, as well as dramatically increase the drag at high polymer extensibility. More recently, Zheng et al. (2013)⁹ incorporated the FENE-P model into a commercial CFD code ANSYS FLUENT via a User Defined Function interface that produces the instantaneous source terms for momentum equations and constitutive equations. This model has been verified for a viscoelastic fluid in symmetric planar sudden expansion geometry. It shows FENE-P model predicted good flow resistance compared to the previous experimental. The encouraging results prove FENE-P rheological model is capable of capturing essential physical processes in turbulent drag reduction studies. Therefore, the FENE-P rheological model was employed throughout the present study.

The aim of present work is two-fold: to develop a subroutine incorporating FENE-P model into commercial CFD software package ANSYS FLUENT¹⁰; and, to investigate the polymer-induced drag reduction in 3-D flow past circular cylinder over a large range of rheological parameters (polymer length, L , 10-150, Weissenberg number, Wi , 0-80) and flow conditions (Reynolds numbers, Re , 300-2000). The data leads to in-depth insights into the role of polymer on the mechanism of drag reduction.

In the sections below, firstly, the governing equations together FENE-P constitutive equation are presented. We then present corresponding computational domain for flow past circular cylinder modelling, and the numerical setup including discretization scheme, convergence criteria and under relaxation factors. This is followed by a presentation of key modeling results and discussion. The final part of this work is devoted to concluding remarks.

2 Methodology

2.1 Governing equations

In the Finite Volume Method framework, the governing equations of unsteady isothermal flow of incompressible fluid consist of a single set of continuity and momentum equations:

$$\frac{\partial u_i}{\partial x_i} = 0 \quad (1)$$

$$\frac{\partial u_i}{\partial t} + \frac{\partial}{\partial x_j} (u_i u_j) = -\frac{\partial p}{\partial x_i} + \frac{\beta}{Re} \frac{\partial^2 u_i}{\partial x_j \partial x_j} + \frac{1-\beta}{Re} \frac{1}{Wi} \frac{\partial \tau_{ij}^p}{\partial x_j} \quad (2)$$

where u and p are the pressure and velocity, respectively, while subscripts i, j and k are the vector components in the i -th, j -th and k -th directions, respectively. The τ_{ij}^p

represents the additional stress induced by elasticity the polymers in the flow. According to the kinetic theory of FENE-P model, the elastic stress term, τ_{ij}^p , is related to a conformation tensor C_{ij} written as:

$$\tau_{ij}^p = \frac{C_{ij}}{1 - \frac{C_{kk}}{L^2}} - \delta_{ij} \quad (3)$$

in which C and L are the polymer conformation tensor and the maximum molecular extensibility in relation to its equilibrium size, respectively. δ is the Kroneker symbol. In the above equation, the trace of conformation tensor C_{kk} cannot extend over the parameter L^2 . The confirmation tensor C_{ij} is positive-definite symmetric (total 6 component for 3D case) and satisfies the following partial differential equation (PDE)

$$\frac{\partial C_{ij}}{\partial t} + u_k \frac{\partial C_{ij}}{\partial x_k} + \Gamma \frac{\partial^2 C_{ij}}{\partial x_k \partial x_k} = C_{ik} \frac{\partial u_j}{\partial x_k} + C_{kj} \frac{\partial u_i}{\partial x_k} - \frac{1}{W_i} \tau_{ij}^p \quad (4)$$

where Γ refers to the constant scalar diffusivity, chosen so that the Schmidt number ($Sc \equiv \nu / \Gamma$, the ratio of momentum diffusivity to scalar diffusivity) closes to 1 for guaranteeing the numerical stability of the scheme. The dimensionless parameters in equations 1, 2 and 4, Weissenberg number (Wi), Reynolds number (Re) and polymer concentration (β), are defined as:

$$Re = \frac{\rho U d}{\mu} \quad (5)$$

$$Wi = \frac{\lambda U}{d} \quad (6)$$

$$\beta = \frac{\mu_s}{\mu_s + \mu_p} \quad (7)$$

Wi number describes the degree of viscoelasticity; Re number refers to the ratio of inertial forces to viscous forces in a flowing fluid; β is written as the ratio of the zero shear-rate viscosity of the solvent (μ_s) to the zero shear-rate viscosity of the total solution ($\mu_s + \mu_p$) and a homogeneous polymer concentration ($\beta = 0.9$) was imposed throughout the flow field. μ_p is the partial viscosity contributed by the polymer. Here, ρ is the solvent density; U and d are the reference velocity and length separately, where the averaged inlet velocity, 1 m/s, and the cylinder diameter were adopted in the present study; λ is the characteristic polymer relaxation timescale.

The viscoelastic constitutive equation (equation 3) and transport equation (equation 4) are incorporated into the commercial code ANSYS FLUENT ver. 15.0. via UDF interface. The UDF contains a set of coupled user-defined scalar transport equations consisting of four customized terms: transient term, convection term, diffusion term, and source term, respectively. In the CFD-based approach used in the simulations reported here, all of the above governing equations are discretized and solved properly. The numerical procedure through a single iteration (going from iteration $n-1$ to n) is described as: evaluate the C_{kk}^{n-1} and guarantee the polymer boundedness, and obtain a value of τ_{ij}^p is obtained at the beginning of each iteration; solve 6 PDEs for C_{ij} using the τ_{ij}^p from previous step; solve simultaneously continuity equation and momentum

equation using C_{ij} from previous step; update the C_{kk}^n at the end of each iteration. The final solution provides the instantaneous velocity, pressure, polymer conformation, and non-Newtonian stress fields of a fluid with a dilute concentration of polymer additives.

2.2 Problem formulation

The flow past a circular cylinder is one of the classical problems of fluid mechanics since it includes many important physical features such as flow separation, boundary layers, wakes and vortex dynamics, as illustrated in Figure 2. Therefore, it was chosen in the present work to study the complex viscoelastic effect under various flow conditions.

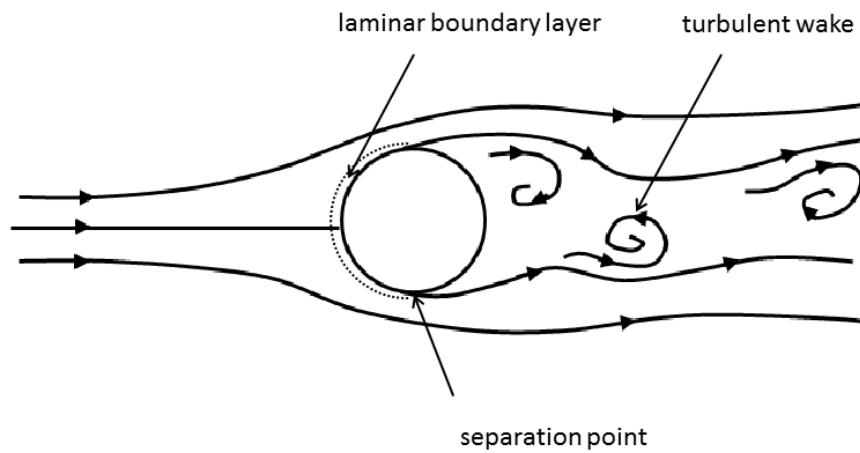
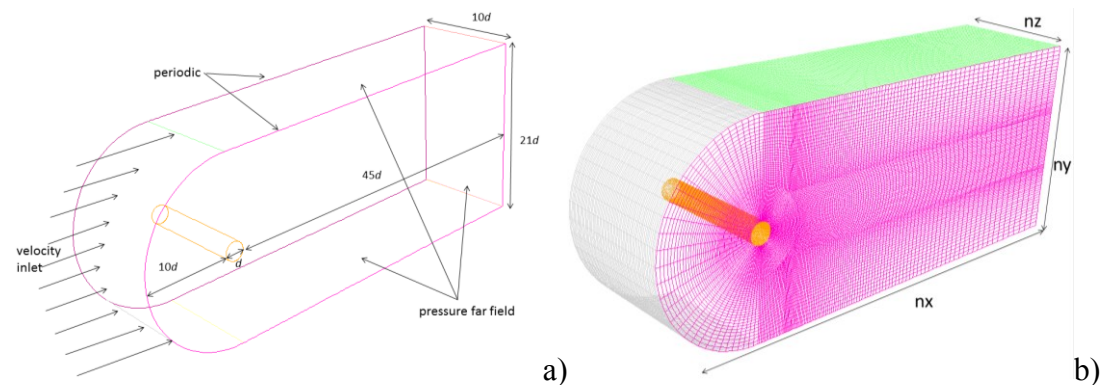


Figure 2 Basic feature of subcritical flow past a circular cylinder¹¹

A circular cylinder of diameter d is placed in an otherwise undisturbed uniform crossflow ($U_\infty = 1.0$ m/s) as shown in Figure 3a). The domain extends radially to $10d$ upstream of the cylinder. The lateral boundaries and the exit boundary in the streamwise direction are placed at $10d$ and $45d$ from the center of the circular cylinder, respectively. The discretization points were 150 and 100 for the streamwise direction and lateral direction separately, see Figure 3b). The spanwise domain length was set at $10d$ and discretized using 50 nodes in order to capture the three-dimensional flow behavior. An oblique view of cylinder wall surface grid is given in Figure 3c). A close-up of the spanwise-normal plane of the unstructured grid surrounding the cylinder is shown in Figure 3d).



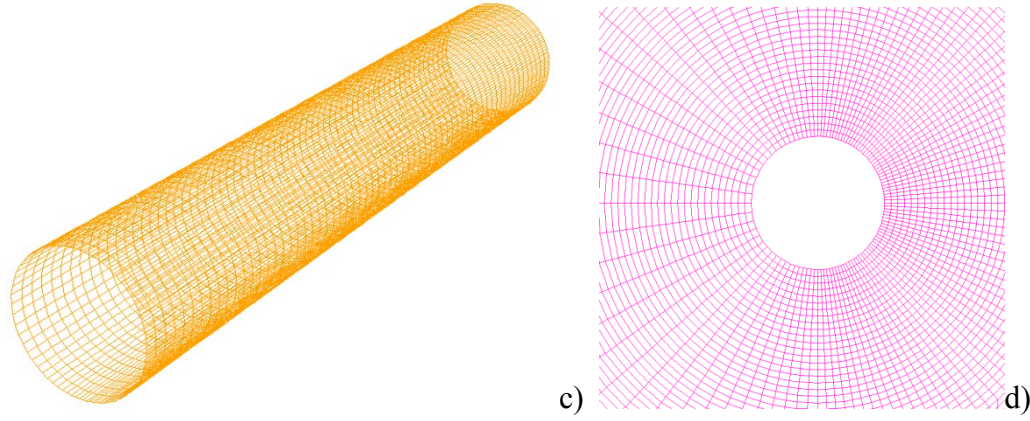


Figure 3 Three-dimensional computing domain, a) geometry of the domain showing the location of cylinder, b) unstructured hexahedral grids (number of nodes $n_x \times n_y \times n_z = 150 \times 100 \times 50$), c) oblique view of circular cylinder, d) close-up of unstructured grid surrounding the cylinder

The boundary condition of entrance is set to be velocity inlet. Two lateral boundaries in spanwise direction were imposed as periodic condition to mimic an infinitely long cylinder. All exits are set as pressure far-field, and the cylinder wall has no-slip boundary condition. The velocity of whole flow field is initialized by the average velocity at the inlet velocity ($u_x = 1 \text{ m/s}$, $u_y = 0$, $u_z = 0$), and the conformation tensor is initialized to be $C_{xx} = C_{yy} = C_{zz} = 1$, and $C_{xy} = C_{yz} = C_{xz} = 0$.

We followed suggestions outlined in recent research⁹ on how to setup the spatial discretization on each governing equation. Pressure implicit with splitting of operators (PISO) scheme is adopted to solve the coupling of velocity and pressure; standard scheme is utilized to discretize the pressure equation; QUICK scheme is used to discretize the momentum equation and user-defined-scalar equations. The second order implicit method was used to advance the solution in time. The convergence criteria are set as small as 10^{-6} and under relaxation factors are tightened to 0.02 for all variables. The time step is set to be 0.001 s and a maximum number of 20 iterations for each time step. All of the transient simulations running for flow time up to 2000 s were conducted on a HP-Z820 24-core 3.4 GHz workstation run in parallel.

3. Results and discussion

It was necessary to validate and benchmark CFD's ability to predict the flow structure. A suitable case with Newtonian flow ($Re = 195$) was therefore performed prior to the broad tests on non-Newtonian flows. The CFD predicted streamline pattern colored by velocity magnitude were then compared with the experiments¹². As shown, both CFD and experiment captured the classic von Karman vortex street occurring behind the cylinder. It was also found that the flow begins to separate from the wall surface where the reverse flow occurred.

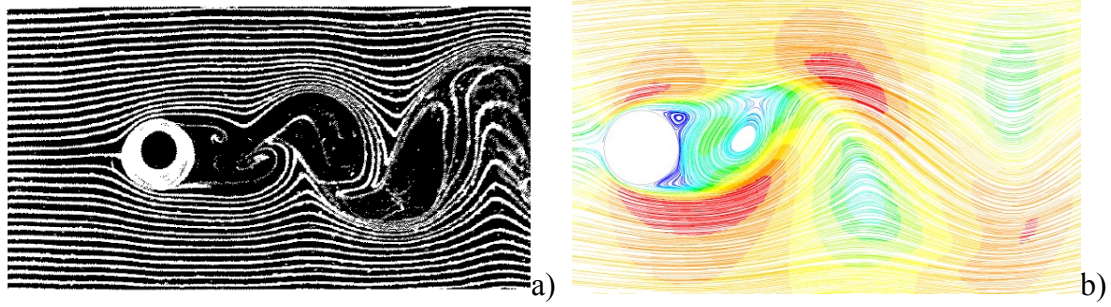


Figure 4 Comparison of the streamlines between the experimental¹² data and the CFD modeling.

After confirming the predictive capability of the present CFD code, the same analysis was done for the viscoelastic flows to obtain an overall insight into the polymer-induced drag reduction. Ideally, the numerical modelling needs cover a broad range of rheological parameters and flow conditions, which requires a considerable amount of computing resources and makes the work impossible. Therefore, 3 value of each parameter (L : 10, 30 and 100; Wi : 0, 10 and 80; Re : 300, 1000 and 2000) has selected in the present work, see Table 1. Total 9 data points/combinations of Wi , L and Re has been tested in the aforementioned numerical experiments.

Table 1 Test matrix of the numerical experiment, total 8 data points/combination of Wi , Re and L , and keep polymer concentration, c , as constant, $c = \frac{1}{\beta} - 1 \approx 0.1$, representing the typical dilute solutions.

Case Number	Re	Wi	L
1	300	0 (Newtonian)	10
2	300	10	10
3	300	80	10
4	300	10	30
5	300	10	100
6	300	10	150
7	1000	10	10
8	2000	10	10

A baseline case (Case 2) for non-Newtonian flow past cylinder has been tested and the development of 3D flow patterns was displayed in Figure 5. One can see a pair of symmetric counter-rotating vortices generated behind the cylinder and develops further on as time elapsing. All other cases discussed henceforth were compared with the baseline cases.

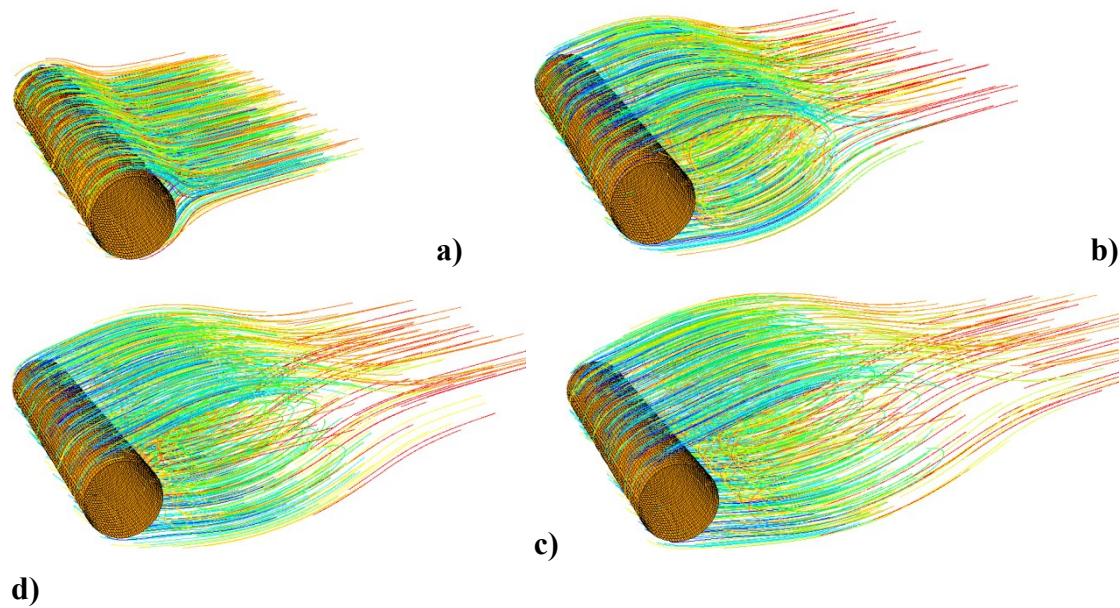
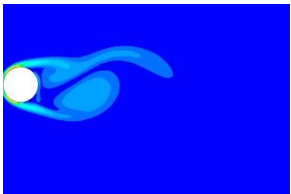
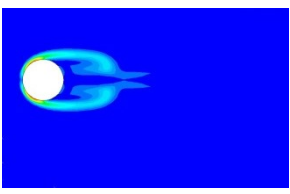
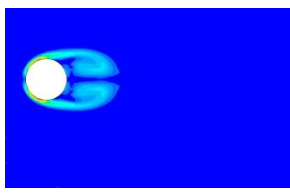


Figure 5 Development of flow pattern for a non-Newtonian flow past cylinder (baseline case): a) $t = 100$ s, b) $t = 200$ s, c) 400 s, d) 600 s.

3.1 Influence of Weissenberg number

To investigate the influence of fluid elasticity on the flow patterns, numerical simulations with Wi number ranging from 0 (Newtonian) to 80 have been conducted, at fixed Reynolds number, 300, and finite-extensibility, 10. For comparative purposes, the contours of vortex shedding patterns are plotted at the same time instants for different cases, see Figure 6. One can see that strong and periodic vortex shedding has been observed for both elastic and inelastic fluids. At first, a pair of symmetric vortices formed behind the cylinder. As flow develops, one of the two vortices breaks away and then the second is shed due to the non-symmetric pressure in the wake region.

As shown, the non-Newtonian cases exhibit a longer recirculation region behind the cylinder compared to those obtained by Newtonian flow due to their greater resistance to normal deformations. The greater Wi value is, the stronger the fluid elasticity is, and a larger recirculation region is. Since normal strains are resisted more intensively by elastic fluids, a retardation of the vorticity development is observed for the case with a higher Wi value. The pronounced retardation can be seen over the early stage of flow development, 200- 600s.

Wi	0 (Newtonian)	10	80
time			
100 s			

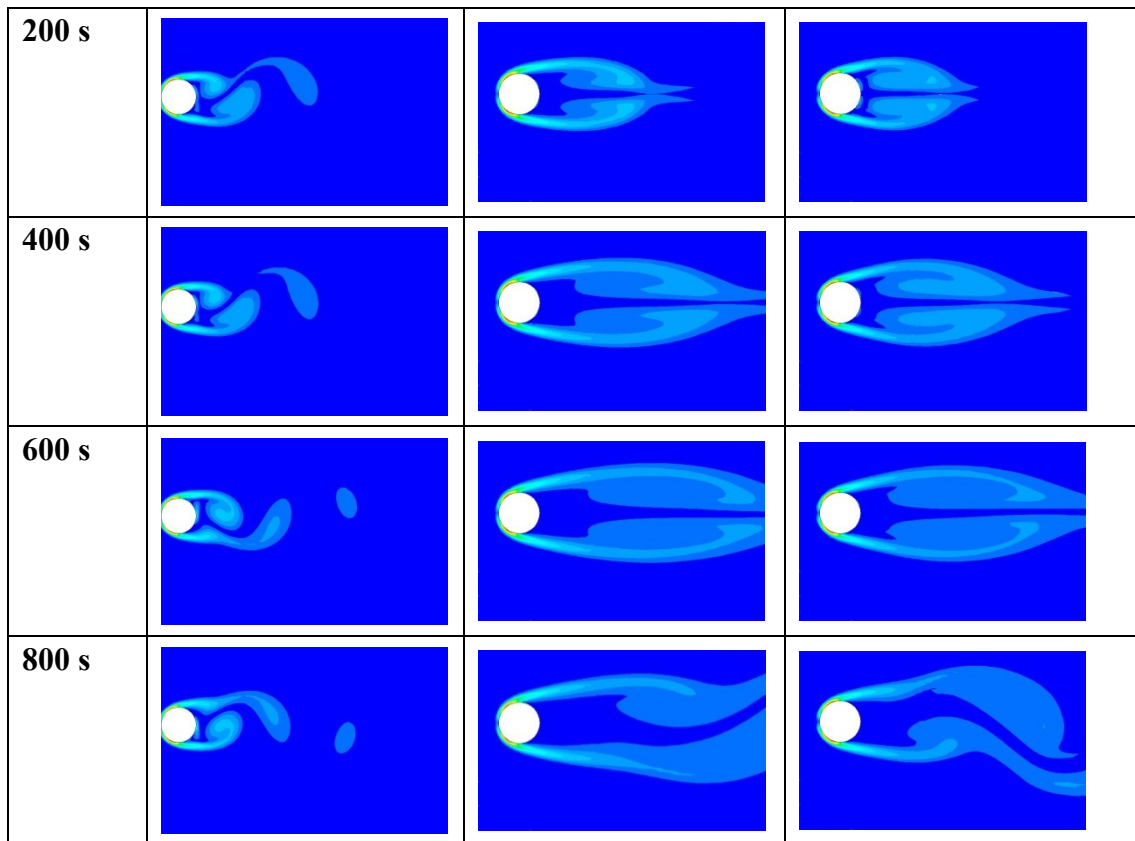
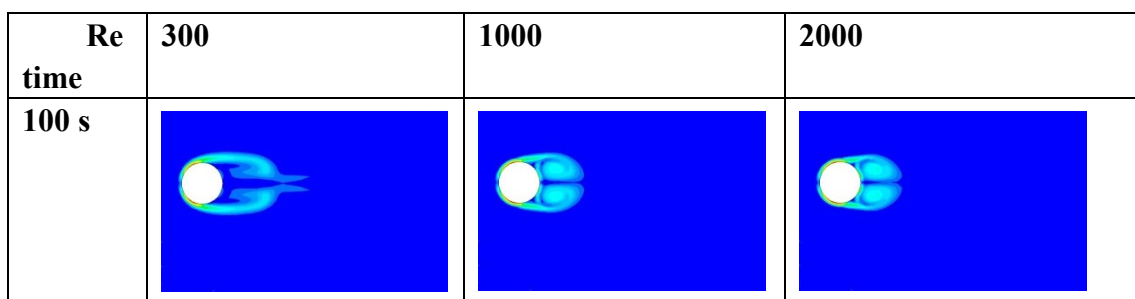


Figure 6 Influence of Weissenberg number (Wi) on the vorticity field of visco-elastic flow past cylinder, $Re = 300$, $L = 10$.

3.3 Influence of Reynolds number

To study the influence of Re number on flow patterns, numerical simulation were conducted by varying Re (300-2000) at constant Wi number, 10, and L value, 10. The instantaneous contour of vorticity field was illustrated for different Re numbers in Figure 7, which shows that the lasting period of vortices reduces as Re number increases. This is because the flow with high Re number exhibits stronger inertial forces causing unsteady vortex shedding. In addition, increasing Re number causes the boundary layer transitioning ahead of separation, which is more resistant to separation, hence effectively move the separation point downstream, see the contours at 800s.



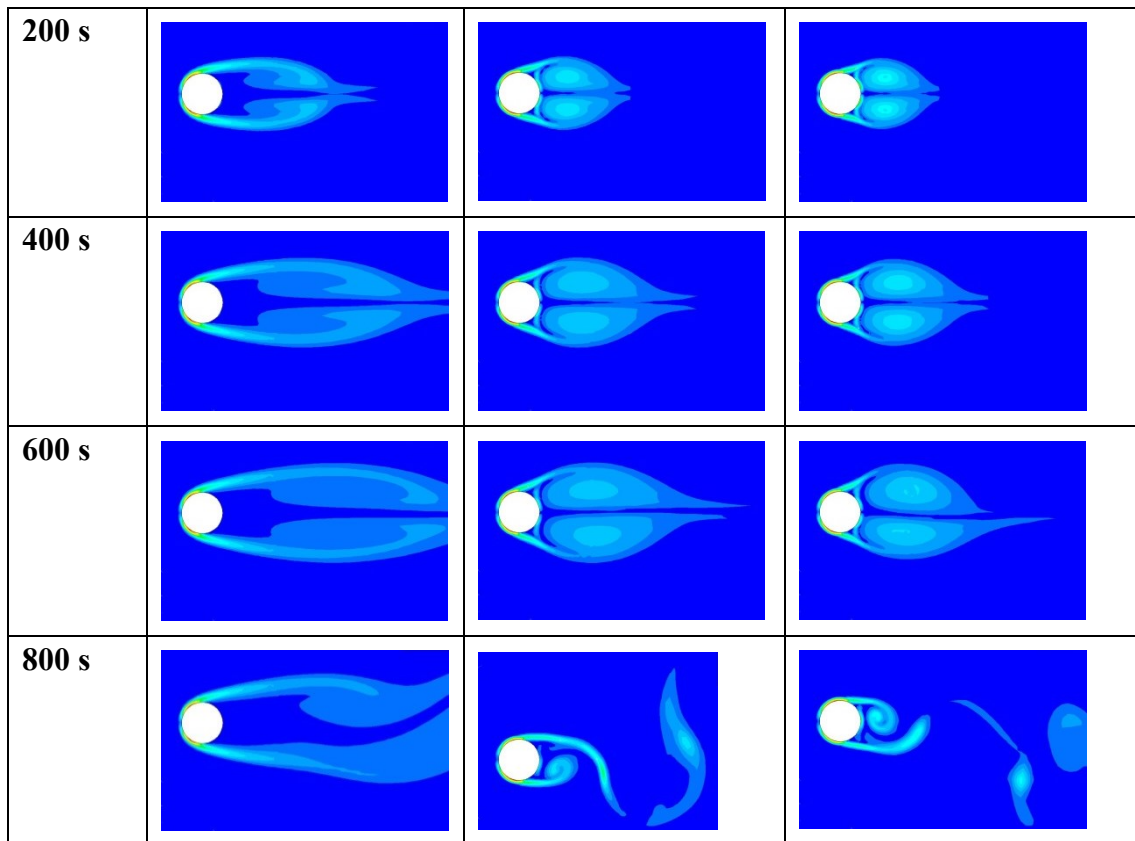
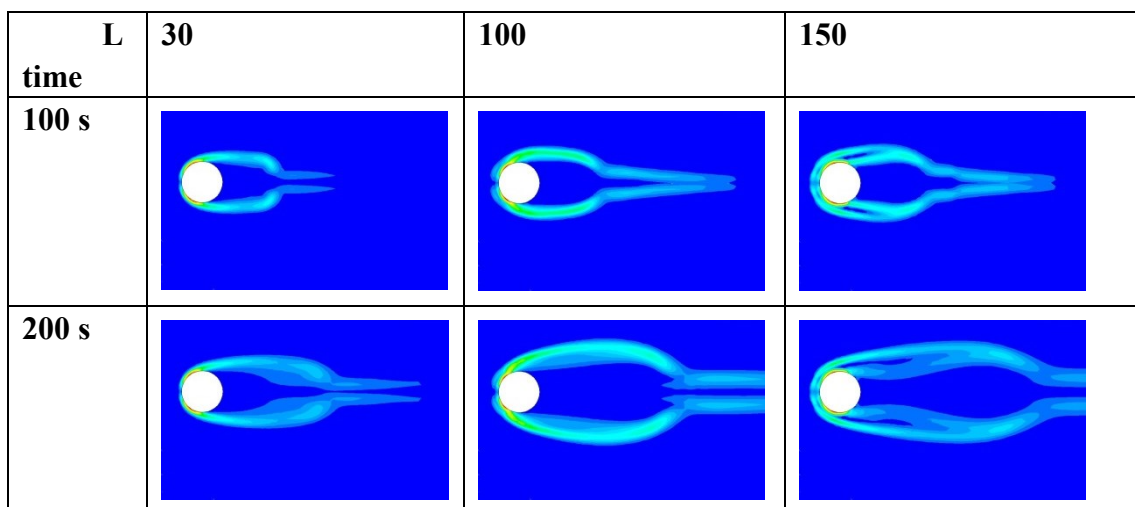


Figure 7 Impact of Reynolds number (Re) on the vorticity field of visco-elastic flow past cylinder, $Wi = 10$ and $L = 10$.

3.4 Influence of finite extensibility parameter

The influence of polymer extensibility on flow pattern was illustrated in Figure 7. Total 4 maximum extensibility values ($L = 10, 30, 100$ and 150) have been selected for comparative purpose. The instantaneous contour of vorticity fields clearly shows larger L value weakens the streamwise vortices and elongates the recirculating region behind the cylinder along with an upstream shifting of the flow separation point. The contours also indicate larger extensibility tends to delay the growth of instabilities.



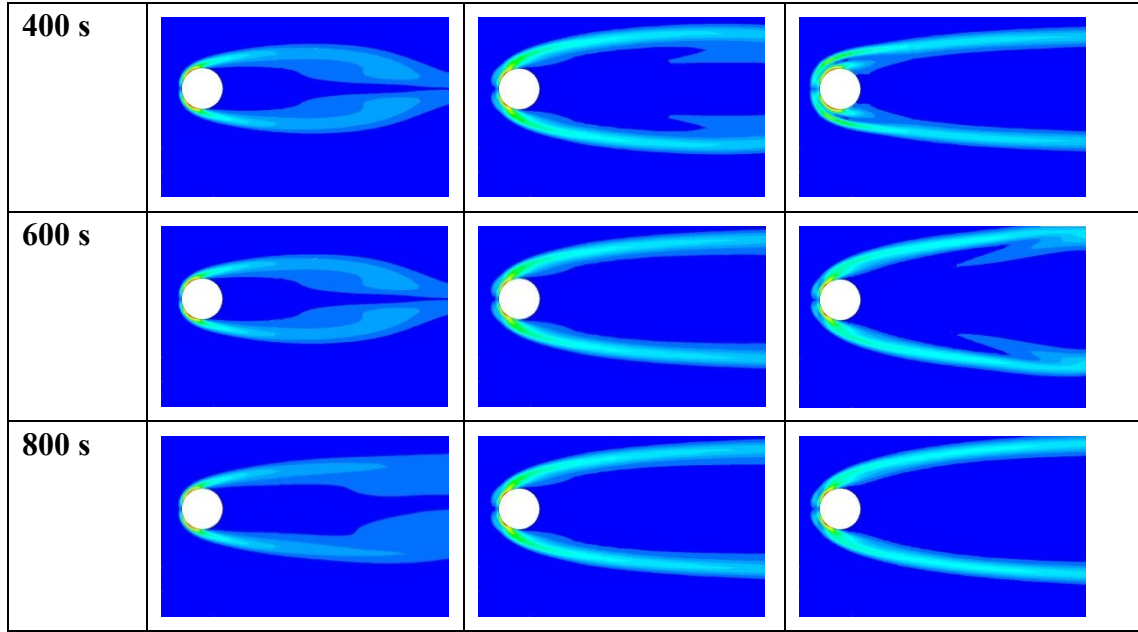


Figure 7 Impact of molecular extensibility (L) on the vorticity field of visco-elastic flow past cylinder, $Re = 300$, $Wi = 10$.

3.5 Quantitative Analysis

To obtain a quantitative view of the aforementioned influences, various quantities (e.g. the drag coefficient, Strouhal number) have been calculated and used for comparing the results. Drag coefficient is defined as the ratio of the drag force to the force produced by the dynamic pressure times the area, written as:

$$C_D = \frac{F_d}{\frac{1}{2}\rho U^2 A} = \frac{\oint P \hat{n} \cdot \hat{e}_d dS + \oint \tau_w \hat{t} \cdot \hat{e}_d dS}{\frac{1}{2}\rho U^2 A} \quad (8)$$

where F_d is the drag force consisting of a pressure term ($\oint P \hat{n} \cdot \hat{e}_d dS$) and a viscous term ($\oint \tau_w \hat{t} \cdot \hat{e}_d dS$), ρ the fluid density, U the reference velocity and A the frontal area of the cylindrical tube. An example of the temporal evolution of drag coefficients for viscoelastic flow past a cylinder is given in Figure 8 a). And an example of dimensionless pressure ($P/\rho U^2$) profile over cylinder is given in Figure 8 b). As shown, the pressure on the front of the cylinder is near the stagnation pressure which is much higher than that in the back side of the cylinder.

The Strouhal number reflecting the vortices shedding frequency is defined by

$$S_t = \frac{f_r d}{U} \quad (9)$$

where f_r is the shedding frequency, d and U the diameter of circular cylinder and reference velocity. To accurately calculate the shedding frequency, the lift coefficient history was recorded. By taking an average of 10 shedding cycles (e.g. 10 C_L peak as shown in Figure 8 b)), the shedding frequency could be calculated as

$$f_r = \frac{10}{t_2 - t_1} \quad (10)$$

where t_1 and t_2 are the time when the first and tenth C_L peaks appear.

It is evident from the Figs 8a) and c) that the oscillations of drag and lift coefficients

show clear sinusoidal patterns. The averaged C_L equals zero, while the averaged C_D returns a positive value larger than zero. The frequency of drag coefficient oscillates at twice the frequency of the lift coefficient, i.e. shedding frequency. The viscoelastic fluid flow exhibits a lower the drag amplitude and temporal-averaged drag coefficient.

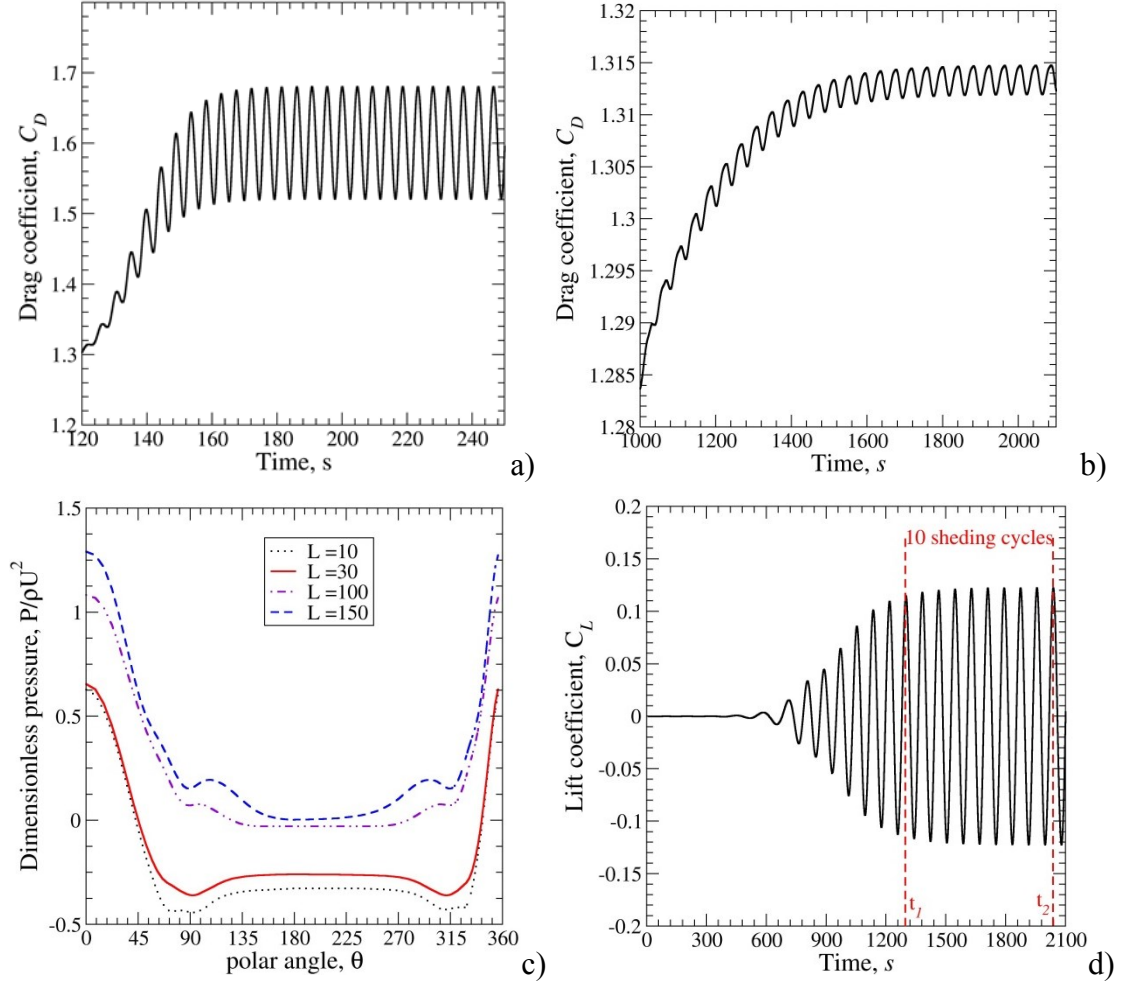


Figure 8 Examples of a) temporal evolution of drag coefficient of Newtonian flow, b) temporal evolution of drag coefficient of viscoelastic flow (baseline model), c) dimensionless pressure profile over a cylinder (baseline model), and d) lift coefficients for viscoelastic flow past a circular cylinder. Polar angle θ in b) measured counterclockwise from leading edge stagnation point.

The influence of Wi , Re and L on averaged drag coefficient is plotted quantitatively in Figure 9. In general, the averaged drag coefficient decreases, $\sim 30\%$ drag reduction, as polymer viscoelasticity Wi increases from 0 to 80 and hold Re and L as constant at 300 and 10. This decrease resulted from a rising base pressure on the rear portion of the cylinder, which integrated over the surface of the cylinder, results in a diminished form drag¹³. This result indicates effective drag reduction requires high Wi number.

The striking drag reduction, about 50% C_D decrease, was observed as Re number

increases from 300 to 2000 for viscoelastic flow. It shows a trend similar to data for the Newtonian case from Faith A. Morrison (2013)¹⁴. This effect can be explained that laminar boundary layer around the cylinder grows rapidly as Re number increases modestly. The thicker laminar boundary layer is, the wider the flow separation area is, leading a higher base pressure behind the upstream cylinder and hence reduced drag.

The influence of polymer extensibility is more complicated. For low polymer extensibilities ($L = 10-30$), the drag decrease about 20% compared to the Newtonian value, $C_D = 1.53$. For larger polymer extensibilities ($L = 100$ and 150), however, the drag actually increases about 20% compared to the Newtonian case, at constant Wi and Re . This $\pm 20\%$ difference in drag reduction between low and high extensibilities could be explained by analyzing the pressure distribution over the cylinder. For the low extensibility cases, a rising base pressure on the back side of the cylinder is dominated and the back pressure alters slightly. For high extensibility cases, an increase in the leading stagnation point pressure is dominated, even though the back pressure increases modestly, see Figure 8b).

This drag increase for high extensibility has also been seen experimentally¹⁵ and numerically⁸ in which a similar substantial increase in drag was observed for different polymer solutions. However, the contradictory finding that high polymer extensibility favors drag reduction was also reported in experimental¹⁶ and numerical¹⁷ studies.

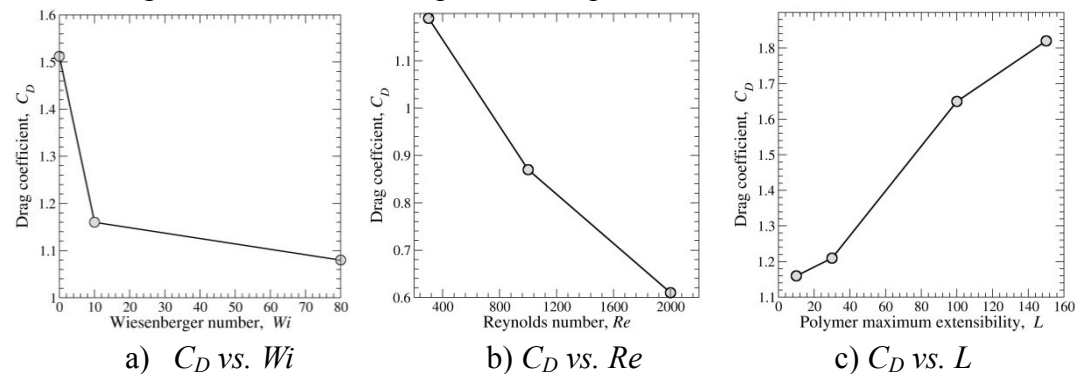


Figure 9 Influence of a) maximum extensibility, b) Reynolds number, c) Weissenberg number on the averaged drag coefficient using the same parameters as Figures 5-7, respectively.

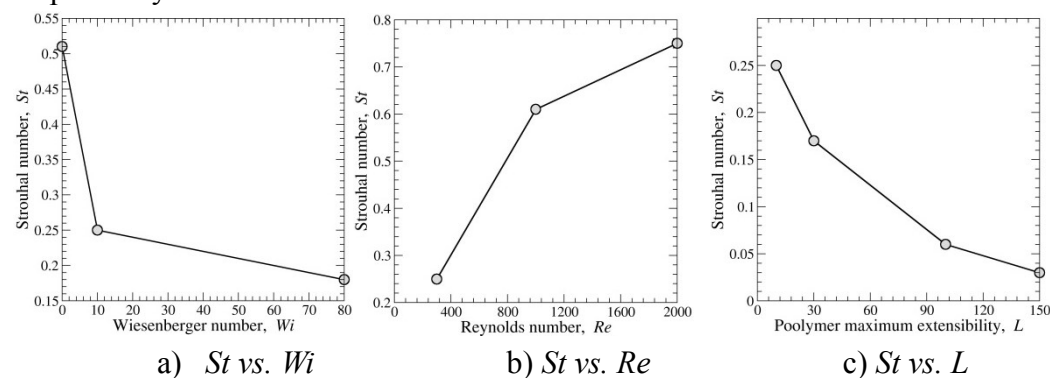


Figure 10 Influence of a) maximum extensibility, b) Reynolds number, c) Weissenberg number on the Strouhal number, St , using the same parameters as

Figures 5-7, respectively.

The influence of Wi , Re and L on dimensionless vortex shedding frequency is plotted as St vs. Wi , St vs. Re and St vs. L , shown in Figure 10. As can be seen, a reduction in vortex shedding frequency (reduced St number) with increasing elasticity (Wi number and L) is in agreement with those reported in the literature. As reported by Sahin and Owens (2004)¹⁸, this decrease as the stabilizing nature of viscoelasticity on the shear layer that develops as fluid flows over the cylinder surface.

Furthermore, the Strouhal number of viscoelastic fluid increases as the Re number increases gradually and reaches a certain “saturation” level around $St \sim 0.75$ (for $Re=2000$), which is much higher than that of classical Newtonian flow past a cylinder, 0.21. The cause of increased shedding frequency at higher Re number results from three-dimension wake instabilities¹⁹ becoming energetic as the inertial forces start to dominate over viscous forces. It was speculated that the “saturated” Strouhal number is associated with the transitioning of complex flow structures. However, the sufficient evidence are still lacking, and the in-depth view of three-dimension vortex structure for high Reynolds number needs to be explored further.

4. Conclusion

In the present work, the flow features of viscoelastic flow past 3D circular cylinder have been simulated and analyzed to obtain in-depth understanding the underlying mechanism of polymer-induced drag reduction. To take into account the elastic stress term induced by polymer stretch, the FENE-P was incorporated into the commercial CFD software via User Defined Function interface. The influence of rheological parameters (i.e. polymer finite-extensibility, L , and Weissenberg number, Wi) and flow conditions (Reynolds number, Re) on the extent of drag reduction and vortices shedding frequency were investigated by means of the Navier-Stokes system. The drag coefficients, Strouhal numbers and vorticity contours have been demonstrated and compared for a broad range of Wi , Re and L values. In light of these results, the main conclusions are drawn here.

It was found that the higher Wi numbers (i.e. longer polymer relaxation time) elevate the extent of drag reduction. This elevated drag reduction was also observed for a modest increase in the polymer finite-extensibility ($L = 10-30$). This elevated drag reduction is attributable to the stabilized cylinder wakes induced by the polymer elasticity. For the high extensibility ($L = 100 -150$) cases, the drag force increases since the pressure profile in the upstream side of cylinder increase dramatically. The drag coefficient increases monotonically as Reynolds number increases.

In addition, the role of polymer elasticity in reducing tStrouhal number (i.e. lowering vortices shedding frequency) is significant compared to Newtonian flow. This reduction effect becomes more pronounced for stronger elasticity (i.e. larger Wi number and L value). Increasing Reynolds number prompted the vortices shedding

frequency and the Strouhal number tends to level off (at $Re = 2000$) probably due to the transition of complex flow structure.

Although the present modeling framework for viscoelastic fluid flow has been comprehensively tested and proved to be a useful tool for simulating the polymer-induced drag reduction, there is still considerable scope for improvement for the future work. For instance, at the highly turbulent flow regime, the turbulence itself can be modelled properly using certain closure models, $k-\epsilon$ or $k-\omega$. However, the sophisticated interplay between Reynolds stress and elastic stress needs to be adapted accordingly. The rational and strategic closure methods have to be developed for this work.

Acknowledgements

The author wishes to acknowledge Shell for financial support.

References

1. Virk P. S. Drag reduction fundamentals. *AIChE J.* 21, 625–56 (1975).
2. White, C. M. and Mungal, M. G. Mechanics and Prediction of Turbulent Drag Reduction with Polymer Additives. *Annu. Rev. Fluid Mech.* 40, 235–56 (2008).
3. Dentoonder, J. M. J., Hulsen, M. A., Kuiken, G. D. C. & Nieuwstadt, F. T. M. Drag reduction by polymer additives in a turbulent pipe flow: numerical and laboratory experiments. *J. Fluid Mech.* 337, 193–231(1997).
4. Bird, R. B., Armstrong, R. C., and Hassager, O. in *Dynamics of polymeric liquids*, vol. 1. (Wiley, 1987).
5. Oliveira, P. J. Method for time-dependent simulations of viscoelastic flows: vortex shedding behind cylinder. *Journal of Non-Newtonian Fluid Mechanics.* 101, 113–137 (2001).
6. Sahin, M. and Owens, R.G. On the effects of viscoelasticity on two-dimensional vortex dynamics in the cylinder wake. *Journal of Non-Newtonian Fluid Mechanics*, 123, 121–139 (2004).
7. Keunings, R. On the high weissenberg number problem. *Journal of Non-Newtonian Fluid Mechanics*, 20, 209–226 (1986).
8. Richter, D., Shaqfeh, E. S. G. and Iaccarino, G. Floquet stability analysis of viscoelastic flow over a cylinder. *J. Non-Newtonian Fluid Mech.* 166, 554–565 (2011).
9. Zheng, Z. Y., Li, F. C. and Yang, J. C. Modeling Asymmetric Flow of Viscoelastic

- Fluid in Symmetric Planar Sudden Expansion Geometry Based on User-Defined Function in FLUENT CFD Package. *Advances in Mechanical Engineering*. 2013, 1-13 (2013).
10. ANSYS® Academic Research, Release 15.0, Help System, “ANSYS ICEMCFD Manual,” ANSYS, Inc., 2014.
 11. Davenport, W.J. “Flow Past a Circular Cylinder”, Virginia Tech University. Available: www.aoe.vt.edu (Accessed: 1 Feb 2016).
 12. Van Dyke, M. In *An album of fluid motion*. (The Paraboloid Press, 1982) 28.
 13. Coelho, P.M. and Pinho, F.T. Vortex shedding in cylinder flow of shear-thinning fluids. III Pressure measurements. *J. Non-Newtonian Fluid Mech.* 121, 55–68 (2004).
 14. Morrison, F. A. In *An Introduction to Fluid Mechanics*, (Cambridge University Press, 2013).
 15. D. James and O. Gupta. Drag on circular cylinders in dilute polymer solutions. Chemical Engineering Progress Symposium Series, 67(111):62–73, 1971.
 16. Cadot, O. and Lebey, M. Shear instability inhibition in a cylinder wake by local injection of a viscoelastic fluid. *Physics of Fluids*. 11(2), 494–496 (1998).
 17. Li, C. F., Sureshkumar, R. and Khomami, B. Influence of rheological parameters on polymer induced turbulent drag reduction. *J. Non-Newtonian Fluid Mech.* 140, 23–40 (2006).
 18. Sahin, M. and Owens, R. G. On the effects of viscoelasticity on two-dimensional vortex dynamics in the cylinder wake. *Journal of Non-Newtonian Fluid Mechanics*, 123, 121–139 (2004).
 19. Cadot, O. and Kumar, S. Experimental characterization of viscoelastic effects on two- and three-dimensional shear instabilities. *Journal of Fluid Mechanics*, 416, 151–172 (2000).